NUCL SCI TECH (2020) 31:99
https://doi.org/10.1007/s41365-020-00812-8

Intrinsic background radiation of $LaBr_3(Ce)$ detector via coincidence measurements and simulations

Hao Cheng[1,2,3] · Bao-Hua Sun[1,2] · Li-Hua Zhu[1,2] · Tian-Xiao Li[3] · Guang-Shuai Li[1] · Cong-Bo Li[3] · Xiao-Guang Wu[3] · Yun Zheng[3]

Received: 11 July 2020 / Revised: 20 August 2020 / Accepted: 22 August 2020 / Published online: 9 October 2020

Abstract The $LaBr_3(Ce)$ detector has attracted much attention in recent years because of its superior characteristics compared with other scintillating materials in terms of resolution and efficiency. However, it has a relatively high intrinsic background radiation because of the naturally occurring radioisotopes in lanthanum, actinium, and their daughter nuclei. This limits its applications in low-counting rate experiments. In this study, we identified the radioactive isotopes in the $\phi 3'' \times 3''$ Saint-Gobain B380 detector by a coincidence measurement using a Clover detector in a low-background shielding system. Moreover, we carried out a Geant4 simulation of the experimental spectra to evaluate the activities of the main internal radiation components. The total activity of the background radiation of B380 is determined to be 1.523 (34) Bq/cm^3. The main sources include ^{138}La at 1.428 (34) Bq/cm^3, ^{207}Tl at 0.0135 (13) Bq/cm^3, ^{211}Bi at 0.0136 (15) Bq/cm^3, ^{215}Po at 0.0135 (3) Bq/cm^3, ^{219}Rn at 0.0125 (12) Bq/cm^3, ^{223}Fr at 0.0019 (11) Bq/cm^3, ^{223}Ra at 0.0127 (10) Bq/cm^3, ^{227}Th at 0.0158 (22) Bq/cm^3, and ^{227}Ac at 0.0135 (13) Bq/cm^3. Of these, the activities of ^{207}Tl, ^{211}Po, ^{215}Po, ^{223}Fr, and ^{227}Ac are deduced for the first time from the secular equilibrium established in the decay chain of ^{227}Ac.

Keywords $LaBr_3$ · Coincidence measurement technique · Intrinsic radiation · GEANT4 simulation

1 Introduction

As a new type of inorganic scintillator, the $LaBr_3(Ce)$ crystal has a high density of 5.08 g/cm^3, a high light output of approximately 63 photons/keV γ, a fast decay time of approximately 16 ns [1], and a good temperature response. These superior characteristics make $LaBr_3(Ce)$ ideal for many applications [2–6] in environmental monitoring, oil well logging, nuclear safeguards, and medical imaging. Thus, $LaBr_3(Ce)$ is often used as a substitute for the widely used NaI(TI) crystal when high performance is required. The integrated $LaBr_3(Ce)$ detector consists of a crystal coupled directly to a photomultiplier tube (PMT). Previous studies of $LaBr_3(Ce)$ detectors [1, 7–14] show excellent linearity in the γ ray response, a good energy resolution of less than 3% (FWHM) for the 662 keV γ ray for a size of up to $\phi 3'' \times 3''$, and an excellent time resolution of approximately $\sim$300 ps (FWHM). The latter has made possible a fast timing detector array composed of $LaBr_3(Ce)$ [15, 16] that is pursued worldwide for nuclear structure studies.

Conversely, the $LaBr_3(Ce)$ detector has a relatively high intrinsic background radiation [11, 17–21], which is typically at least 1 to 2 orders of magnitude higher than that of

This work was supported by the National Key R & D program of China (No. 2016YFA0400504) and by the National Natural Science Foundation of China (Nos. U1832211, U1867210, 11922501, 11961141004, 11575018, 11790322, and U1932209).

✉ Bao-Hua Sun
bhsun@buaa.edu.cn

Li-Hua Zhu
hulh@buaa.edu.cn

[1] School of Physics, Beihang University, Beijing 100191, China

[2] Beijing Advanced Innovation Center for Big Data-Based Precision Medicine, School of Medicine and Engineering, Beihang University, Beijing 100191, China

[3] China Institute of Atomic Energy, Beijing 102413, China

the NaI(Tl) detector. The self-radiation root in ^{138}La and the five short-lived progeny of ^{227}Ac impurities may cause a non-negligible effect in the energy spectrum as a result. This would seriously limit its application in low-count rate experiments such as those with space γ rays. Therefore, it is valuable to quantify the intrinsic radiation of $LaBr_3(Ce)$ and to understand its influence.

The present study aims to identify the components of internal radiation in $LaBr_3(Ce)$ and to deduce their activities. The detector of interest is the Saint-Gobain B380 with a size of $\phi 3'' \times 3''$. This experiment is performed by combining coincidence measurement with dedicated Geant4 simulation. The remainder of this paper is organized as follows. Section 2 presents the coincidence measurement of $LaBr_3(Ce)$ vs. a Clover detector, and the corresponding results. In Sect. 3, we performed Geant4 simulations of the experimental spectra of both $LaBr_3(Ce)$ and the Clover detector, and we deduce the activity of ^{138}La , ^{221}Bi, ^{219}Rn, ^{223}Ra, and ^{227}Th. A summary is provided in Sect. 4.

2 Internal radiation of $LaBr_3(Ce)$ and coincidence measurement

2.1 Internal radiation of $LaBr_3(Ce)$ detector

The internal radiation in the $LaBr_3(Ce)$ crystal has two origins: the naturally occurring radioisotope ^{138}La and the ^{227}Ac impurity. Together, they can decrease the detection sensitivity of γ rays with energies up to approximately 2.5 MeV. A better understanding of self-activity is essential for designing experiments.

^{138}La is the only naturally occurring radioactive isotope of lanthanum, with 0.09% abundance and a half-life of 1.02×10^{11} years, which affects the energy spectrum below 1.5 MeV. ^{138}La decays in two parallel processes, as shown in Fig. 1. 34.4% of the isotope undergoes β^- decay, with a maximum energy of 263 keV, eventually to the first excitation state of ^{138}Ce. This process is associated with the emission of a 788.742-keV γ ray. The remaining 65.6% of ^{138}La disintegrates by electronic capture (EC). This process results in stable ^{138}Ba with the emission of a 1435.795-keV γ ray and the characteristic X-rays of Ba with energies ranging from 31 to 38 keV.

^{227}Ac is the grand-daughter nuclide in the ^{235}U decay chain. Because of its similarity in chemistry to lanthanum, it presents as a contaminator with a half-life of 21.77 in $LaBr_3(Ce)$. Figure 2 shows the decay chain down to the stable ^{207}Pb by emitting α, β, and γ rays. This includes 6 α emitters (^{227}Ac, ^{227}Th, ^{223}Ra, ^{219}Rn, ^{215}Po, and ^{211}Bi) and 4 β emitters (^{227}Ac, ^{211}Pb, ^{211}Bi, and ^{207}Tl). ^{227}Ac and its daughter nuclei produce a higher energy background by emitting α particles, and they also contribute to the β continuum up to approximately 1400 keV as a result of the β decay of ^{211}Pb and ^{207}Tl in the decay chain of this nucleus.

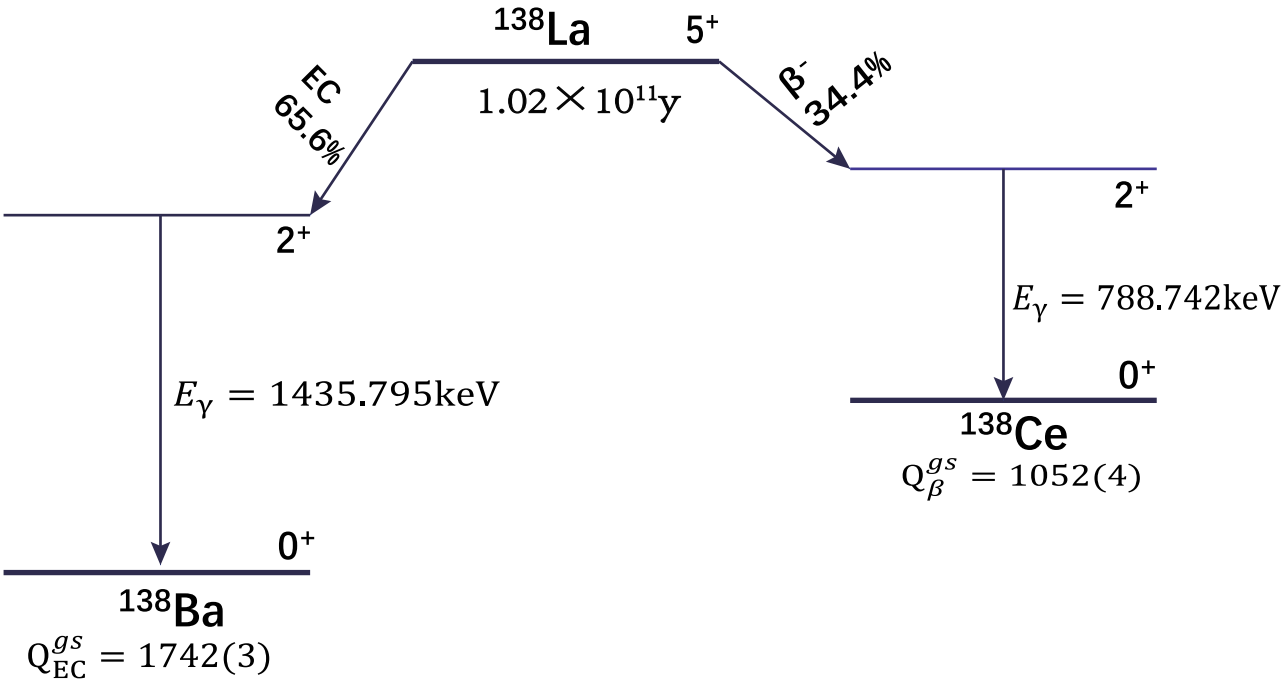

Fig. 1 Decay scheme of ^{138}La. Data are from NNDC [22]

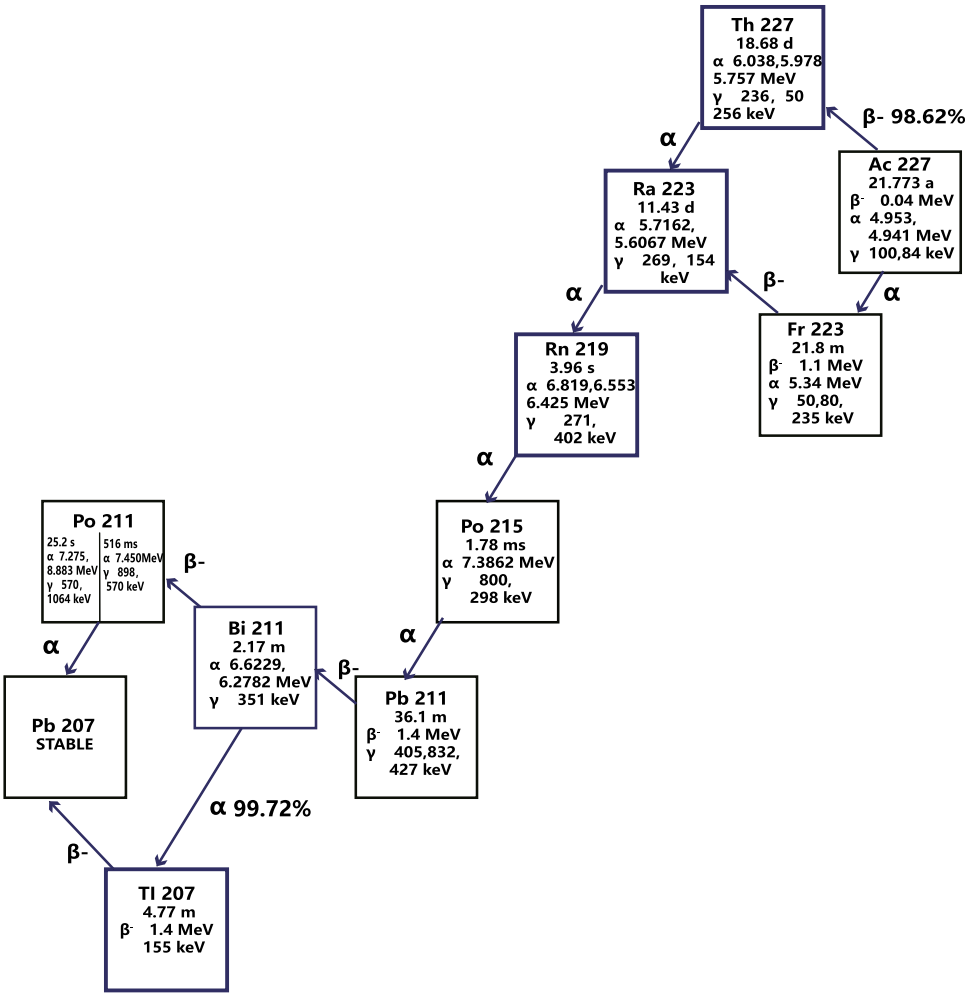

Fig. 2 Actinide decay chain. The half-life, energies of α and characteristic γ rays with relatively high intensities, and β-decay end-point energy for each nuclide. Data are from NNDC [22]

2.2 Experimental setup

Coincidence measurement using an HPGe was conducted in a low-background counting system (LBS). The environmental background counting rate was 58 per second. The LBS is a cylinder with a radius of 64 cm and a height of 66.1 cm, and it consists of four layers: iron, lead, copper, and plexiglass, from the outside to the inside. A schematic diagram of the entire detection system is shown in Fig. 3. The lead layer can shield most of the low-energy environment background, and the purpose of the copper layer is to absorb the characteristic X-rays of lead.

The $LaBr_3(Ce)$ detector is the Saint-Gobain B380 with a $\phi 3'' \times 3''$ crystal. A high-purity germanium (HPGe) Clover detector from Canberra was placed directly facing the $LaBr_3(Ce)$. The high voltage applied to the $LaBr_3(Ce)$ detector was set to 520 V. A higher voltage may cause electron saturation in the photomultiplier, affecting linearity [23] in the energy determination. The Clover consists of four coaxial N-type high-purity germanium detectors, each with a diameter of 60 mm and length of 60 mm. The energy resolutions for the $LaBr_3(Ce)$ and Clover were measured to be 2.1% (FWHM) and 0.166% (FHWM) for a 1.332-MeV γ ray, respectively. The relative efficiency was 38% for each germanium crystal.

The energy and time signals of the two detectors were acquired using the VME data acquisition system and collected for 37,187 s in total. Dead time correction and time stamps were added to the data acquisition software. Standard radioactive sources ^{60}Co, ^{137}Cs, and ^{241}Am were used for the γ-ray energy calibration up to approximately 1.33 MeV. The calibration accuracy was cross-checked using the characteristic γ-rays of ^{138}La. Moreover, to calibrate the high-energy spectrum of $LaBr_3(Ce)$, we used the recoil-electron energies from the Compton scattering process of 2.615-MeV γ rays of ^{208}Tl, a naturally radioactive nuclide in an environmental background. Such calibration is only possible using the coincidence measurement with Clover.

2.3 Coincidence measurement

The intrinsic radiation of the $LaBr_3(Ce)$ scintillator was identified by coincidence measurement using the

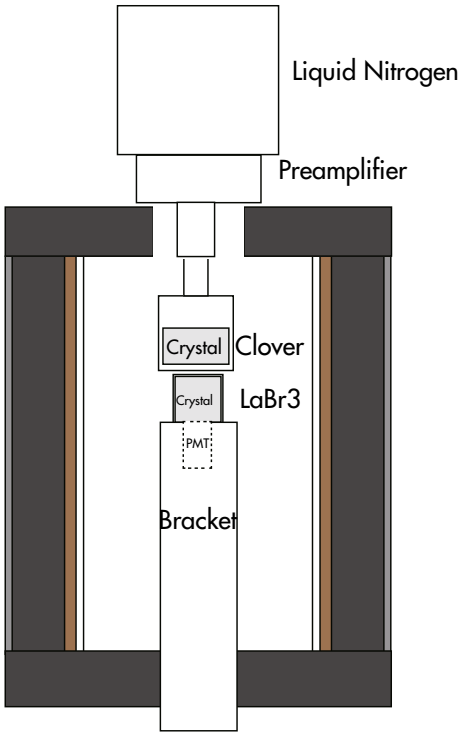

Fig. 3 (Color online) Schematic diagram of experimental setup. It contains $LaBr_3$ and Clover crystals and a low-background shielding room. The shielding room is composed of plexiglass, copper, lead, and iron from the inside to the outside. The $LaBr_3$ detector is supported by a bracket in a shielded room

$LaBr_3$(Ce) and Clover detectors. The relevant background spectra after energy calibration are shown in Fig. 4. In the self-counting spectrum of $LaBr_3$(Ce), we first see a low-energy peak centered at approximately 35.5 keV. This is attributed to the sum of 95.6% of the 31.83 keV K_α X-ray response and 90% of the 5.6 keV Auger electron response in the EC decay process, by referring to the theoretical calculation [20]. The energy shift is due to the non-proportional response of the $LaBr_3$(Ce) crystal. Then, we see a β continuum with an end point of 263 keV mixed with the Compton continua, primarily from the 788.7 and 1435.8 keV of ^{138}La and the 1460.8 keV of ^{40}K. With increasing energy, the 788.7 keV bump is shown to extend to higher energies and end at approximately 1 MeV. This is due to the coincidence of the 788.7-keV γ with the β^- continuum. The 1435.8-keV γ-rays produced by the EC of ^{138}La coincided with the 32-keV X-rays of ^{138}Ba and the 1460.8-keV γ-rays of ^{40}K, resulting in a double peak near 1461 keV, as shown in Fig. 4a.

The spectrum above 1.8 MeV shows a three-peak structure, revealing the presence of α emitter contaminants. Although the α energies from ^{227}Ac and its daughter nuclei are as high as 5.0–7.4 MeV (see Fig. 2), the energies are read out in the spectrum calibrated with γ-rays to be in the energy range of 1.5 and 2.5 MeV because of the well-known light quenching effect (see, for example Ref. [18]).

The energy spectrum of the Clover detector, as well as the coincidence spectrum, is shown in Fig. 4b. It is clear that the characteristic γ-rays of 788.7 keV and 1435.8 keV

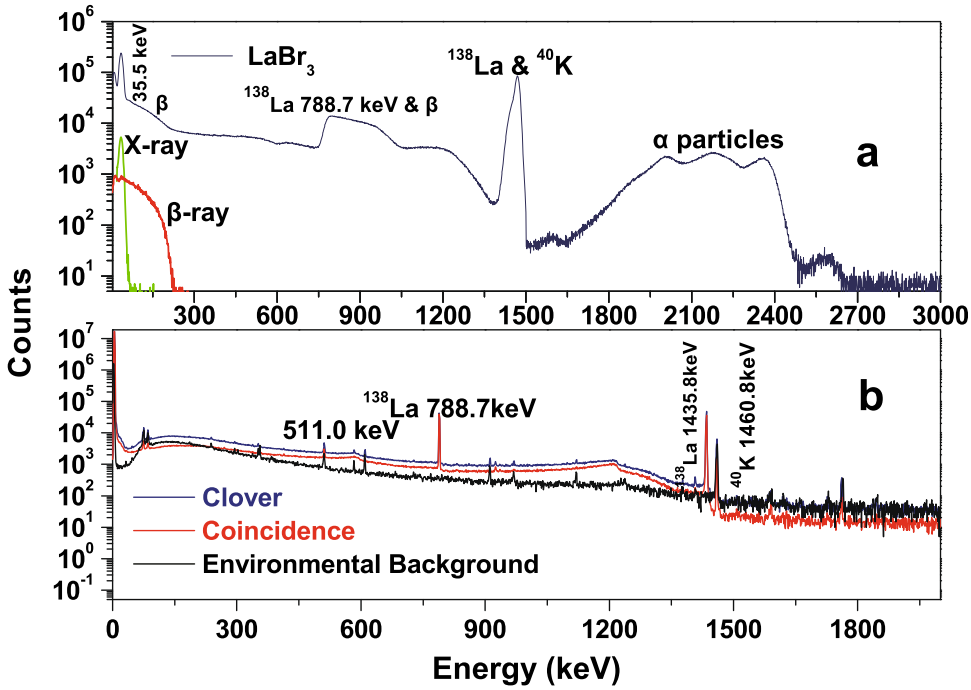

Fig. 4 (Color online) Background radiation spectra measured for 37,187 s by the $LaBr_3$(Ce) detector (**a**) and the Clover (**b**). The coincidence β spectrum (red) and X-ray spectrum (green) in the $LaBr_3$(Ce) detector are shown in (**a**). The coincidence spectrum (red) and environmental background spectrum (black) of the Clover are shown in (**b**). For details, refer to the text

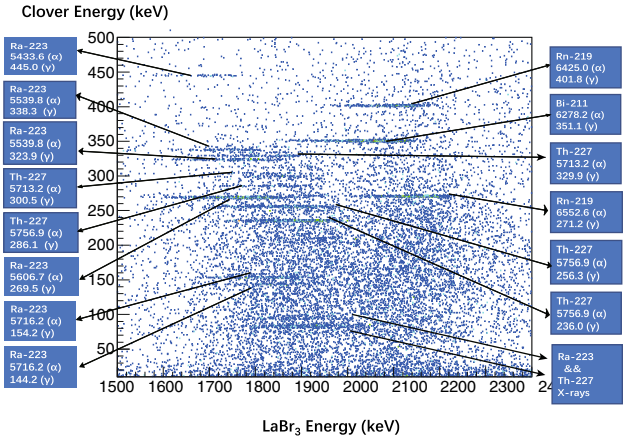

Fig. 5 (Color online) Matrix of the $LaBr_3(Ce)$ versus Clover. Listed are also the events of $\alpha - \gamma$ correlations and the identified radioactive isotopes. Both detectors were calibrated with characteristic γ-rays. The events between 1.5 and 2.4 MeV for $LaBr_3$3(Ce) correspond to 5–7.4 MeV α particles of the ^{227}Ac decay chain. See the text for details

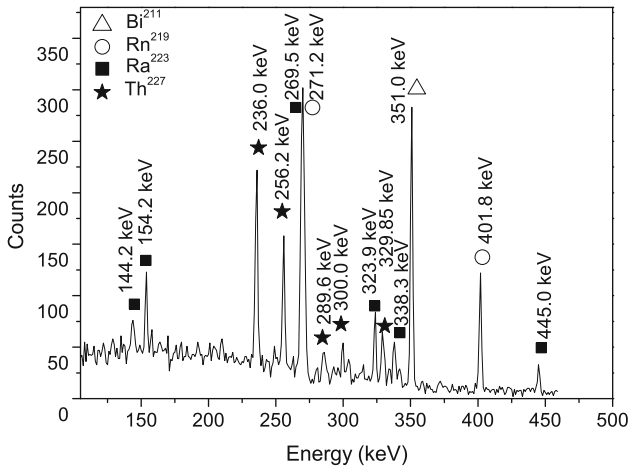

Fig. 6 Projected γ-ray energy spectrum of Fig. 5 in the Clover. Labeled are the identified nuclei

of ^{138}La decays were enhanced and the environmental background was further reduced in the coincidence spectrum. Setting gates in the Clover spectrum at 788.7 keV and 1435.8 keV of ^{138}Ba decays allows us to pick up the β spectrum and the X-ray spectrum in the $LaBr_3(Ce)$ detector, as shown in Fig. 4a]. The coincidence β spectrum has triggered a precise study of ^{138}La decay [20, 24–27], which is a second forbidden unique decay. The β and X-ray distributions are shown for comparison in the $LaBr_3(Ce)$ spectrum.

Part of the coincidence events in the Clover and $LaBr_3(Ce)$ detectors are displayed in Fig. 5, while the projection to the Clover is shown in Fig. 6. The horizontal bands in Fig. 5 are traced back to the α-γ cascades. The

Table 1 α-γ coincidences identified in ^{227}Th, ^{223}Ra, ^{219}Rn, and ^{211}Bi

Isotope	$\alpha_{E_\gamma}E_\alpha$ (keV)	Shown in Fig. 5.
^{227}Th	$\alpha_{236}5757$	√
^{227}Th	$\alpha_{256}5757$	√
^{227}Th	$\alpha_{286}5757$	√
^{227}Th	$\alpha_{300}5713$	√
^{227}Th	$\alpha_{329}5713$	√
^{227}Th	$\alpha_{61}5977$	–
^{227}Th	$\alpha_{334}5709$	–
^{223}Ra	$\alpha_{144}5716$	√
^{223}Ra	$\alpha_{154}5716$	√
^{223}Ra	$\alpha_{270}5607$	√
^{223}Ra	$\alpha_{324}5540$	√
^{223}Ra	$\alpha_{338}5540$	√
^{223}Ra	$\alpha_{445}5434$	√
^{223}Ra	$\alpha_{127}5747$	–
^{219}Rn	$\alpha_{402}6425$	√
^{219}Rn	$\alpha_{271}6553$	–
^{219}Rn	$\alpha_{402}6425$	–
^{211}Bi	$\alpha_{351}6278$	√

Listed are the $\alpha_{E_\gamma}E_\alpha$ and whether it is present in Fig. 5. E_γ and E_α are the energies of the γ ray and coincident α, respectively

correlated γ ray energies and their relative intensities are key to identifying the α emitters.

The α emitters identified by the $\gamma - \alpha$ coincidence are ^{227}Th, ^{223}Ra, ^{219}Rn, and ^{211}Bi. This is consistent with previous investigations of $LaBr_3(Ce)$ with a size of $\phi 1'' \times 1''$ [9] and $LaCl_3(Ce)$ with a size of ϕ25mm $\times$25mm) [17]. The main γ-rays and α emitted by ^{227}Th, ^{223}Ra, ^{219}Rn, and ^{211}Bi are shown in Table 1. Some α values listed in the table cannot be seen in Fig. 5 because their branches are relatively low. The α (6.038 MeV from ^{227}Th, 6.62 MeV from ^{211}Bi, and 6.82 MeV from ^{219}Rn) with relatively high intensity cannot be seen in Fig. 5 because the parent nucleus decays to the ground state of the daughter nucleus. The third peak in the single spectrum of $LaBr_3(Ce)$ in Fig. 4a is the 7.386 MeV α line from the ground state of ^{215}Po to the ground state of ^{211}Pb, in which there is no cascade γ-ray.

3 Discussion

In this section, we will deduce the activity of various radioactive contaminations embedded in $LaBr_3(Ce)$. Because radioactive contaminants are evenly distributed in the crystal, it is practically impossible to make a direct determination because of the lack of accurate efficiency calibration for both detectors.

Table 2 Details of shielding materials of the LBS

Layer	Inner radius (cm)	Outer radius (cm)	Material
Iron	30	32	G4_Fe
Lead	21.65	30	G4_Pb
Copper	21.45	21.65	G4_Cu
Plexiglass	20.95	21.45	G4_PLEXIGLASS

The material layer, inner radius, outer radius, and materials defined in Geant4 are listed

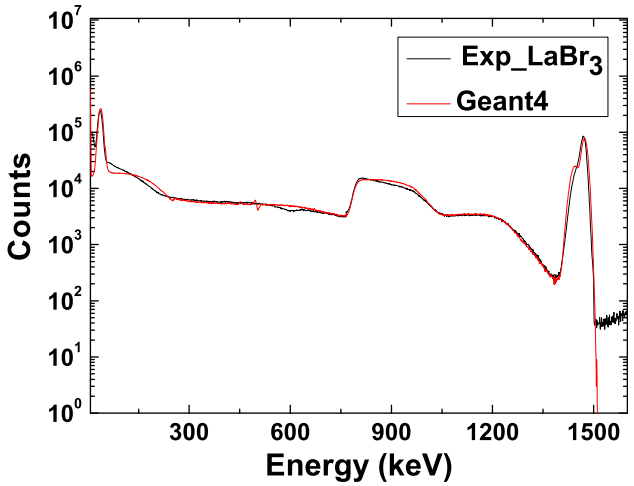

Fig. 7 (Color online) Comparison of experimental (black line) and simulated (red line) self-counting energy spectra in the $LaBr_3$ detector. The sampling of simulation was scaled to the experimental data collected for 37,187 s

Instead, in this work, we develop a Monte Carlo model based on the Geant4 version 10.4 [28–30] toolkit. The setup includes the Clover, the $LaBr_3$(Ce) detector as well as its bracket, and all components of the shielding system, as shown in Fig. 3. ^{138}La isotopes are evenly distributed in the $\phi 3'' \times 3''$ cylindrical $LaBr_3$ crystal. The density of the $LaBr_3$ (Ce) crystal was set to 5.08 g/cm^3 [1]. We employed the physics constructor class of G4EmStandardPhysics [30]. It includes various processes, such as the deposition of β and γ rays in the sensitive volumes of the detectors, the occurrence of Compton scattering in the shield, and the characteristic X-rays induced from the shield material. The shielding materials are summarized in Table 2. The activities of ^{138}La and ^{227}Ac decay chain contaminators were determined by reproducing the experimental spectra in both the $LaBr_3$(Ce) and Clover detectors.

3.1 Simulation of the self-counting $LaBr_3$(Ce)

We compare the simulation with the experimental data acquired at the same measurement time, that is, 37,187 s. The best fit to the experimental spectrum is found using the least squares method when the activity of ^{138}La 482(19) Bq corresponds to 1.396 (55) Bq/cm^3. This corresponds to 180,030,639 decays of ^{138}La over 37,187 s in total. The uncertainty quoted here is due to the experimental statistics, detection efficiency, and branching ratio of the γ-rays. The experimental and simulated spectra are plotted in Fig. 7. Good agreement is seen, except for the low-energy part up to approximately 150 keV. To reproduce the experimental spectrum, we adopted the following function [31] for the γ-ray energy (E_γ) resolution (η):

$$\ln(\eta) = -\frac{1}{2} \times \ln(E_\gamma) - 3.82\,. \quad (1)$$

It should be noted that in the above simulation, we did not consider the contribution from ^{227}Ac and its daughter nuclei. This may partially account for the difference between the simulation and experimental spectra. Another possible reason for the low-energy deficiency in the simulation could be insufficient understanding of the β decay of ^{138}La. This has been discussed in Ref. [24–27].

3.2 Activities determined using the Clover data

An alternative way to deduce the ^{138}La activity is to use the coincidence γ ray information at 788.7 and 1435.8 keV in Clover. This would require an accurate efficiency calibration of the Clover detector using a volume source of the

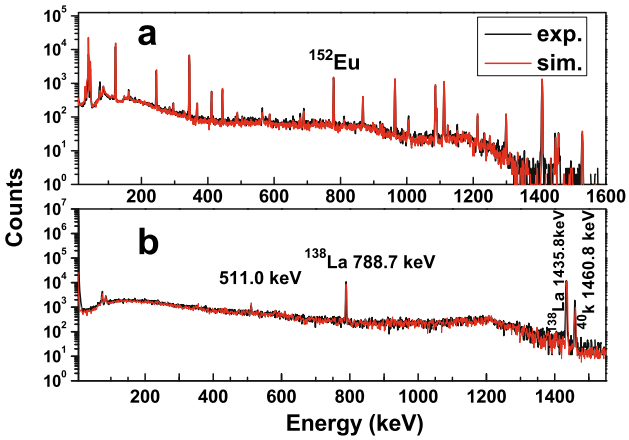

Fig. 8 (Color online) Comparison of Clover spectrum (black line) with simulation (red line) for a ^{152}Eu source (**a**) and $LaBr_3$(Ce) crystals (**b**). The sampling of the simulation for $LaBr_3$(Ce) was scaled to the experimental data collected for 37,187 s

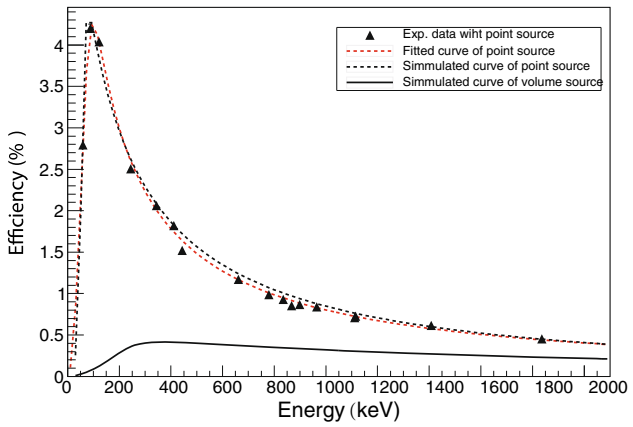

Fig. 9 (Color online) γ-ray detection efficiencies of Clover. The red dashed line is the fitting curve for the experimental data (solid triangle) from the standard point source, while the black dashed line is the simulation efficiency under the same detection configuration. The black solid line represents the detection efficiency when the source is evenly distributed in the $LaBr_3(Ce)$ crystal

same volume as the $LaBr_3(Ce)$ detector, which is practically impossible.

In reality, we performed a two-step optimization of the calibration [32]. In step one, we followed the standard routine for efficiency calibration using the standard radioactive point sources ^{137}Cs, ^{241}Am, ^{54}Mn, ^{88}Y, ^{109}Cd, ^{65}Zn, and ^{152}Eu. These sources are selected to avoid a possible true summing effect. The point source was placed 3 cm from the front surface of the Clover detector. We used the EFFIT program in the software package [33] to describe the efficiency curve for the low-energy and high-energy regions separately.

In this step, we optimized the thickness of the dead layer encapsulating the crystal by the least squares method to best reproduce the Clover spectrum of ^{152}Eu. The best simulation results of the ^{152}Eu spectrum together with the experimental data are presented in Fig. 8a. The simulated detection efficiency curve was compared with the experimental results using a standard point source, as shown in Fig. 9.

In step two, we modeled the detection efficiency of the Clover with sources evenly distributed in the $LaBr_3(Ce)$ crystal, instead of point sources. The simulated efficiency curve is shown in Fig. 9. The efficiency of 788.7 keV and 1435.8 keV γ-rays were determined to be 0.00347(11) and 0.00257(10), respectively. In the simulation, the interaction of characteristic γ-rays with both the $LaBr_3(Ce)$ and Clover detectors and even the shielding material were taken into account.

As a result, we found that the Clover spectrum collected for 37,187 s is best reproduced when the total count of the 788.7-keV γ-ray is 22,423 (164). The simulation and experimental data are shown in Fig. 8b. The activity of ^{138}La is thus extracted to be 504 (16) Bq, corresponding to 1.451 (58) Bq/cm^3. The uncertainty takes into account the contributions from the statistics, detection efficiency, and branching ratio of the γ-rays in the decay of ^{138}La. In the same way, the activity of ^{138}La was also deduced from the 1435.8-keV γ-ray to be 500 (20) Bq, corresponding to 1.437 (63) Bq/cm^3. Both are consistent with those determined from the self-counting of the $LaBr_3(Ce)$ detector, as shown in Table 3. In fact, the activity of ^{138}La in the $LaBr_3(Ce)$ B380 detector can be estimated according to the natural abundance of ^{138}La, 0.08881(71)% [22], and its half-life $T_{1/2} = 1.02 \times 10^{11}$a. The activity amounts to 1.456(40) Bq/cm^3. This is in good agreement with our measurements.

The above procedure can also be applied to evaluate the activities of the ^{227}Ac decay chain contaminators. In Fig. 6, we identified the characteristic γ-rays at 351.1 keV (^{211}Bi), 271.2 keV and 401.8 keV (^{219}Rn), 269.5 keV and 445.0 keV (^{223}Ra), and 236.0 keV (^{227}Th). The activities of ^{211}Bi, ^{219}Rn, ^{223}Ra, and ^{227}Th are 0.0136 (15) Bq/cm^3, 0.0125 (12) Bq/cm^3, 0.0127 (10) Bq/cm^3, and 0.0158 (22) Bq/cm^3, respectively.

The half-life of the parent radionuclide ^{227}Ac is much longer than the half-life of the daughter radionuclide in the Ac-decay chain. In principle, secular equilibrium should occur, namely, the activities A of each emitter should be equal:

$$A = \lambda_1 N_1 = \lambda_2 N_2 = \lambda_3 N_3 \ldots, \quad (2)$$

where λ_i and N_i are the decay constant and the number of nuclear species i, respectively. Indeed, as shown in Fig. 10, the activities of ^{211}Bi, ^{219}Rn, ^{223}Ra, and ^{227}Th agree well within the error bars. Here, the decay branchings of the ^{227}Ac and ^{211}Bi decay were taken into account. The average activity was computed to be 0.0135(13) Bq/cm^3. The secular equilibrium allows us to determine the activities of all nuclei in the decay chain, namely, ^{207}Tl, ^{211}Po, ^{215}Po, ^{223}Fr, and ^{227}Ac as 1.35×10^{-2}(13), 3.79×10^{-5}(36), 1.35×10^{-2}(13), 1.9×10^{-4}(11), and 1.35×10^{-2}(13), respectively. The results are summarized in Table 3.

We included all of the α emitters in the decay chain, as discussed above, into the Geant4 code, and simulated the 37,187-s energy spectrum. The quenching effect of the α particles and recoil nuclei in the scintillator is not included because of the lack of precise calibration. The results are shown in Fig. 11. The energy resolution of each alpha particle was assumed to be 6%.

One can easily identify a similar pattern of simulations for the experimental high-energy spectrum. This verifies the ^{227}Ac contribution to the energy spectrum of 4.5 MeV to 5.2 MeV, ^{223}Ra and ^{227}Th to the spectrum of 5.2 MeV to 6.5 MeV, ^{211}Bi and ^{219}Rn to the spectrum of 6.5 MeV to

Table 3 Activities of ^{227}Ac decay chain contaminators and ^{138}LaThe isotopes are the most distinct γ rays according to the deduced activities. Results from Refs. [17, 21] are shown whenever available

Isotope	γ-energy (keV)	Absolute efficiency (%)	Activity (Bq/cm^3)	Reference value (Bq/cm^3)
^{211}Bi	351.1	0.4347	$1.36 \times 10^{-2}(15)$	0.032[a]
^{219}Rn	271.2	0.4117	$1.34 \times 10^{-2}(17)$	–
^{219}Rn	401.8	0.4317	$1.16 \times 10^{-2}(16)$	0.032[a]
Average of ^{219}Rn			$1.25 \times 10^{-2}(12)$	–
^{223}Ra	269.5	0.4130	$1.26 \times 10^{-2}(13)$	0.025[a]
^{223}Ra	445.0	0.4283	$1.27 \times 10^{-2}(15)$	–
Average of ^{223}Ra			$1.27 \times 10^{-2}(10)$	–
^{227}Th	236.0	0.3840	$1.58 \times 10^{-2}(22)$	0.037[a]
Sum activity of the above α contaminators			$5.45 \times 10^{-2}(30)$	
^{207}Tl	–	–	$1.35 \times 10^{-2}(13)$	–
^{211}Po	–	–	$3.79 \times 10^{-5}(36)$	–
^{215}Po	–	–	$1.35 \times 10^{-2}(13)$	–
^{223}Fr	–	–	$1.9 \times 10^{-4}(11)$	–
^{227}Ac	–	–	$1.35 \times 10^{-2}(13)$	–
^{138}La	788.7	0.3467	1.451(58)	
^{138}La	1435.8	0.2567	1.437(63)	
^{138}La	Self-counting method		1.396(55)	–
Average activity of ^{138}La			1.428(34)	1.530(70)[b]
Total activity		1.523(34)	–	

[a]Date from Ref. [17],

[b] Date from Ref. [21],

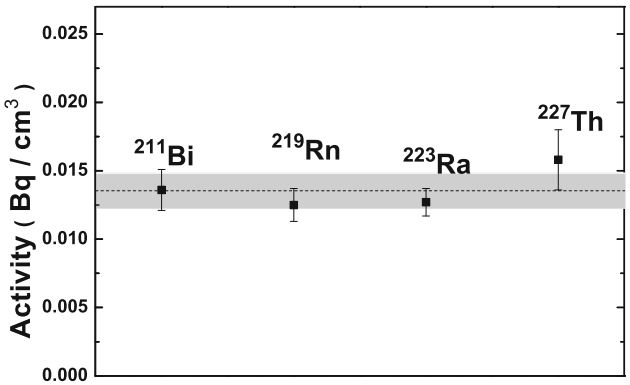

Fig. 10 Activities of ^{221}Bi, ^{219}Rn, ^{223}Ra, and ^{227}Th deduced from the $\alpha - \gamma$ coincidence experiment. The average value and relevant uncertainty are indicated by the shaded area

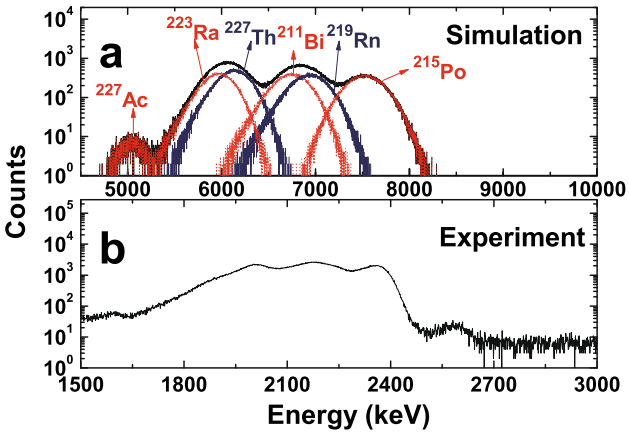

Fig. 11 (Color line) **a** Simulated alpha energy spectrum of the $LaBr_3$(Ce) detector. The contributions from each isotope are labeled. **b** High-energy part of the experimental spectrum. The simulation was scaled to an experimental duration of 37,187 s

7.2 MeV, and ^{211}Po and ^{215}Po to the spectrum of 7.2 MeV to 8.5 MeV. The sum activity of α contaminators is 0.095(4) Bq/cm^3, which is smaller by a factor of 14 than that of ^{138}La.

A similar intrinsic background exists in all of the La-containing crystals. A pioneering study [17] of the $LaCl_3$(Ce) detector with a crystal size of ϕ25 mm $\times$25 mm identified the total α activity of ^{227}Th , ^{221}Bi, ^{219}Rn, and ^{223}Ra as 0.126 Bq/cm^3, and each contribution is summarized in Table 3. In the present study of the B380 type, the ^{227}Ac atom/La atom amounts to 2.0×10^{-12} . The sum activities of ^{227}Th , ^{221}Bi, ^{219}Rn, and ^{223}Ra are typically 40% of that in Ref. [17]. This indicates that the actinium impurity has been significantly reduced in the last decade.

^{138}La and ^{227}Ac impurities resulted in a counting rate (including environmental background) of 237 counts/s for γ-ray energies between 20 and 500 keV, 182 counts/s between 500 and 1.5 MeV, and 27 counts/s above 1.5 MeV in our $LaBr_3$(Ce) detector. Self-irradiation affects its

application to low-production experiments, in particular for potential cases with a count rate of less than 450 counts/s.

4 Summary

In this work, we performed a coincidence measurement using a Clover detector and identified the internal radioactive nuclei of the B380 $LaBr_3(Ce)$ detector. By combining the coincidence spectra with Geant4 simulations, we determined the activity of ^{138}La, ^{211}Bi, ^{219}Rn, ^{223}Ra, and ^{227}Th with good accuracy. Moreover, we found that the secular equilibrium of the ^{227}Ac decay chain is well established in the detector considered here. This allows us for the first time to decouple the activities of ^{207}Tl, ^{211}Po, ^{215}Po, ^{223}Fr, and ^{227}Ac from the spectrum to obtain a complete picture of the intrinsic background from α- and β- decays. These data and the method presented here are useful for designing detector setups based on $LaBr_3$(-Ce), particularly for the purpose of low-count rate experiments.

References

1. https://www.crystals.saint-gobain.com/sites/imdf.crystals.com/files/documents/lanthanum-material-data-sheet.pdf
2. A. Iltis, M.R. Mayhugh, P. Menge et al., Lanthanum halide scintillators: properties and applications. Nucl. Instrum. Methods A **563**, 359–363 (2006). https://doi.org/10.1016/j.nima.2006.02.192
3. J.H. Liu, D.W. Li, Z.M. Zhang et al., Using a $LaBr_3$: Ce scintillator for positron annihilation lifetime spectroscopy. Chin. Phys. C **36**, 380–383 (2012). https://doi.org/10.1088/1674-1137/36/4/016
4. Y.Y. Ji, H.Y. Choi, W. Lee et al., Application of a $LaBr_3(Ce)$ scintillation detector to an environmental radiation monitor. IEEE Trans. Nucl. Sci. **65**, 2021–2028 (2018). https://doi.org/10.1109/TNS.2018.2823322
5. I. Mouhti, A. Elanique, M.Y. Messous et al., Validation of a NaI(Tl) and $LaBr_3(Ce)$ detector's models via measurements and Monte Carlo simulations. J. Radiat. Res. Appl. Sci. **11**, 1687–8507 (2018). https://doi.org/10.1016/j.jrras.2018.06.003
6. C. Cheng, W.B. Jia, D.Q. Hei et al., Determination of thickness of wax deposition in oil pipelines using gamma-ray transmission method. Nucl. Sci. Tech. **29**, 109 (2018). https://doi.org/10.1007/s41365-018-0447-4
7. E.V.D. van Loef, P. Dorenbos, C.W.E. van Eijk, High-energy-resolution scintillator: Ce^{3+} activated $LaCl_3$. Appl. Phys. Lett. **77**, 1467 (2000). https://doi.org/10.1063/1.1308053
8. K.S. Shah, J. Glodo, M. Klugerman et al., $LaBr_3$: Ce scintillators for gamma-ray spectroscopy. IEEE Trans. Nucl. Sci. **50**, 2410–2413 (2003). https://doi.org/10.1109/TNS.2003.820614
9. R. Nicolini, F. Camera, N. Blasi et al., Investigation of the properties of a $LaBr_3$: Ce scintillator. Nucl. Instrum. Methods A **582**, 554–561 (2007). https://doi.org/10.1016/j.nima.2007.08.221
10. F. Quarati, A.J.J. Bos, S. Brandenburg et al., X-ray and gamma-ray response of a $2'' \times 2''$ $LaBr_3$: Ce scintillation detector. Nucl. Instrum. Methods A **574**, 115–120 (2007). https://doi.org/10.1016/j.nima.2007.01.161
11. A. Lavagno, G. Gervino, A. Scarfone, Study of linearity and internal background for LaBr 3: Ce gamma ray scintillation detector. Nucl. Instrum. Methods A **718**, 504–505 (2013). https://doi.org/10.1016/j.nima.2012.11.024
12. M.S. Alekhin, J.T.M. de Haas, I.V. Khodyuk et al., Improvement of gamma-ray energy resolution of $LaBr_3$:Ce^{3+} scintillation detectors by Sr^{2+} and Ca^{2+} co-doping. Appl. Phys. Lett. **102**, 161915 (2013). https://doi.org/10.1063/1.4803440
13. R. Shi, X.G. Tuo, H.L. Li et al., Unfolding analysis of $LaBr_3$: Ce gamma spectrum with a detector response matrix constructing algorithm based on energy resolution calibration. Nucl. Sci. Tech. **29**, 1 (2018). https://doi.org/10.1007/s41365-017-0340-6
14. https://www.crystals.saint-gobain.com/sites/imdf.crystals.com/files/documents/labr-performancesummary-2019.pdf
15. O.J. Roberts, A.M. Bruce, P.H. Regan et al., A $LaBr_3$: Ce fast-timing array for DESPEC at FAIR. Nucl. Instrum. Methods A **748**, 91–95 (2014). https://doi.org/10.1016/j.nima.2014.02.037
16. B. Longfellow, P.C. Bender, J. Belarge et al., Commissioning of the $LaBr_3(Ce)$ detector array at the National Superconducting Cyclotron Laboratory. Nucl. Instrum. Methods A **916**, 141–147 (2018). https://doi.org/10.1016/j.nima.2018.10.215
17. B.D. Milbrath, R.C. Runkle, T.W. Hossbach et al., Characterization of alpha contamination in lanthanum trichloride scintillators using coincidence measurements. Nucl. Instrum. Methods A **547**, 504–510 (2005). https://doi.org/10.1016/j.nima.2004.11.054
18. B.D. Milbrath, J.I. Mcintyre, R.C. Runkle et al., Contamination studies of $LaBr_3(Ce)$ scintillators. IEEE Trans. Nucl. Sci. **53**, 3031–3034 (2006). https://doi.org/10.1109/TNS.2006.881064
19. R. Rosson, J. Lahr, B. Kahn, Radation background in a $LaBr_3$ γ-ray scintillation detector. Health Phys. **101**, 703–708 (2011). https://doi.org/10.1097/HP.0b013e3182211172
20. F.G.A. Quarati, I.V. Khodyuk, C.W.E. Eijk et al., Study of ^{138}La radioactive decays using $LaBr_3$ scintillators. Nucl. Instrum. Methods A **53**, 46–52 (2012). https://doi.org/10.1016/j.nima.2012.04.066
21. A. Camp, A. Vargas, J.M. Fernández-Vareab, Determination of $LaBr_3(Ce)$ internal background using a HPGe detector and Monte Carlo simulations. Appl. Radiat. Isot. **109**, 512–517 (2016). https://doi.org/10.1016/j.apradiso.2015.11.093
22. https://www.nndc.bnl.gov/nudat2/chartnuc.jsp
23. Y.A. Trofimov, E.E. Lupar, V.N. Yurov, Linearity of the energy scale of a detector based on a $LaBr_3(Ce)$ scintillator. Instrum. Exp. Tech. **56**, 151–155 (2013). https://doi.org/10.1134/S0020441213010314
24. A. Giaz, G. Gosta, F. Camera et al., Measurement of β^- decay continuum spectrum of ^{138}La. Europhys. Lett. **110**, 42002 (2015). https://doi.org/10.1209/0295-5075/110/42002
25. F.G.A. Quarati, P. Dorenbos, X. Mougeot, Experiments and theory of ^{138}La radioactive decay. Appl. Radiat. Isot. **108**, 30–34 (2016). https://doi.org/10.1016/j.apradiso.2015.11.080
26. F.G.A. Quarati, P. Dorenbos, X. Mougeot, Reprint of experiments and theory of ^{138}La radioactive decay. Appl. Radiat. Isot. **109**, 172–176 (2016). https://doi.org/10.1016/j.apradiso.2016.01.017
27. R. Sandler, G. Bollen, J. Dissanayake et al., Direct determination of the ^{138}La β^- decay Q value using Penning trap mass spectrometry. Phys. Rev. C **100**, 014308 (2019). https://doi.org/10.1103/PhysRevC.100.014308
28. D.H. Wright, GEANT4-a simulation toolkit. Nucl. Instrum. Methods A **506**, 250–303 (2002). https://doi.org/10.2172/799992
29. J. Allison, K. Amako, J. Apostolakis et al., Geant4 developments and applications. IEEE Trans. Nucl. Sci. **53**, 270–278 (2006). https://doi.org/10.1109/TNS.2006.869826

30. J. Allison, K. Amako, J. Apostolakis et al., Recent developments in Geant4. Nucl. Instrum. Methods A **835**, 186–225 (2016). https://doi.org/10.1016/j.nima.2016.06.125
31. M. Moszynski, M. Kapusta, D.Wolski et al., Energy Resolution of Scintillation detectors with large area avalanche photodiodes and photomultipliers light readout. IEEE Nucl. Sci. Symp **556**, 259-265 (2012) https://doi.org/10.1016/j.nima.2005.09.049
32. L.C. He, L.J. Diao, B.H. Sun et al., Summing coincidence correction for γ-ray measurements using the HPGe detector with a low background shielding system. Nucl. Instrum. Methods A **880**, 22–27 (2018). https://doi.org/10.1016/j.nima.2017.09.043
33. https://radware.phy.ornl.gov/gf3/gf3.html$#$5.3